Monthly Weather Review

VOLUME 98, NUMBER 11

NOVEMBER 1970

UDC 551.513.1:551.509.313 "1959.01"

A STUDY OF THE ENERGETICS OF JANUARY 1959

GASTON PAULIN [1]

Meteorological Service of Canada, Department of Transport, Montreal, Quebec

ABSTRACT

The energetics of the 500-, 100-, and 25-mb levels are computed on a daily and monthly basis during January 1959. On the average, during the month, zonal wave numbers 1 and 2 were dominant in the eddy kinetic and eddy available potential energy spectra at 25 and 100 mb; while at 500 mb, the emphasis was shifted to wave numbers 2 and 3. The dominance of the planetary scale over the synoptic scale at 500 mb was a manifestation of the persistence of a blocking circulation found during the month. The planetary scale tropospheric block had a direct influence on the stratospheric kinetic energy by initiating upward progression of planetary wave energy that in turn was partially absorbed by the stratospheric layers. A 10- to 12-day fluctuation in the blocking circulation was found to be followed by a pulsation of similar frequency in the eddy kinetic energy at 25 mb. Of the three pulses in the block, the second one had the largest amplitude and was followed by a stratospheric warming at 25 mb. The contour pattern at 25 mb during the warming phase was eccentric in character; whereas the other two eddy kinetic energy pulses, before and later, were characteristically of a bipolar nature. At 25 mb, in situ large-scale baroclinic processes contributed significantly to the occurrence and maintenance of the spectral energy maxima. At the same level, a nonnegligible influence of the large-scale kinetic energy mode was provided by the nonlinear wave energy transfers.

1. INTRODUCTION

Earlier studies of the atmosphere's general circulation were aimed at producing a climatological body of knowledge about the energy processes encountered in the atmosphere. These studies were originally conducted to clarify the long-term average mechanisms. It is now possible to describe the energetics of events with better space and time resolution. The discovery of the stratospheric "sudden" warming phenomenon by Scherhag (1952) triggered a whole series of studies on specific major warmings in the years centered around 1960. It was rapidly discovered that a warming was not an isolated phenomenon, as the troposphere played an essential role in the event. The present study investigates the energy behavior of the atmosphere during a more or less normal winter month (January 1959). Furthermore, it emphasizes the daily changes in the energy parameters associated with events at the same or at other levels. The results of this study related to the tropospheric-stratospheric interactions may be of some utility to the most recent general circulation models in which the effects of the stratosphere-troposphere complex are simulated.

In the daily sets, the available data consisted of temperature and height fields at 25, 100, and 500 mb from 30° N. to 80° N. during January 1959. These fields, which had been previously analyzed by visual interpolation, were transformed into zonal Fourier coefficients valid at each 5° of latitude.

2. LIST OF SYMBOLS

K	kinetic energy per unit mass averaged over a constant pressure surface
A	available potential energy per unit mass averaged over a constant pressure surface based on Lorenz (1955)
KZ, KE	zonal and eddy components of K
AZ, AE	zonal and eddy components of A
$KE(n)$	wave number n component of K
$AE(n)$	wave number n component of A
CA	conversion from zonal to eddy available potential energy
CE	conversion of eddy available potential energy into eddy kinetic energy
CK	conversion from zonal kinetic energy to eddy kinetic energy
CZ	conversion of zonal available potential energy into zonal kinetic energy
GZ, GE	zonal and eddy generation of available potential energy

[1] Work done while on educational leave in the Department of Meteorology, McGill University, Montreal, Quebec

CZ^*	computed conversion related to GZ and CZ by $CZ^*=CZ-GZ$
CE^*	computed conversion related to GE and CE by $CE^*=CE-GE$
DZ, DE	zonal and eddy frictional dissipation of kinetic energy
BGZ, BGE	zonal and eddy geopotential flux convergence
$LK(n)$	nonlinear conversion of kinetic energy into the wave number n component from all other kinetic energy components
$LA(n)$	nonlinear conversion of available potential energy into the wave number n component from all other available potential energy components
BAL(XY)	residual needed to balance the budget of an arbitrary energy mode XY
z	height of a constant pressure surface
T	temperature
p	pressure
g	acceleration of gravity
R	gas constant for dry air
f	Coriolis parameter
c_p	specific heat of dry air at constant pressure
σ	static stability factor associated with equation (5), defined as $\sigma=\partial T/\partial p-RT/p\ c_p$
ω	vertical velocity in the p-coordinate system, that is, $\omega=dp/dt$
μ	ratio R/c_p
$J(X, Y)$	Jacobian operator on fields X and Y
$\mathbf{V}$	horizontal wind vector
u, v	eastward and northward components of $\mathbf{V}$
λ, ϕ	longitude and latitude, respectively
$\overline{(\ )}^{\lambda}$	longitudinal averaging operator
$(\ )'$	deviation from the longitudinal average, that is, $(\ )'=(\ )-\overline{(\ )}^{\lambda}$
$\{(\ )\}^{\phi}$	latitudinal averaging operator
$(\ )''$	deviation from the latitudinal average, that is, $(\ )''=(\ )-\{(\ )\}^{\phi}$
$(\ )^*$	deviation from the areal average, that is, $(\ )^*=(\ )-\overline{\{(\ )\}^{\phi}}^{\lambda}$

3. METHODOLOGY

This study follows the concept of available potential energy as formulated by Lorenz (1955) and extended by Muench (1965) and Perry (1966) to be applicable to an open atmospheric layer. The full spectral representation of the energy modes and conversions are fully derived in Perry (1966); an abridged form of the derivation may be found in Paulin (1968). The relevant equations may be found in the appendix.

After omitting details, the four formal energy equations for an individual layer are given in terms of the zonal and eddy forms:

1. The budget for the zonal kinetic energy KZ,

$$\frac{\partial KZ}{\partial t}=BGZ-CK+CZ^*+\mathrm{BAL}(KZ), \tag{1}$$

2. The budget of the eddy kinetic energy KE,

$$\frac{\partial KE}{\partial t}=BGE+CK+CE^*+\mathrm{BAL}(KE), \tag{2}$$

3. The budget of the zonal available potential energy AZ,

$$\frac{\partial AZ}{\partial t}=-CA-CZ^*+\mathrm{BAL}(AZ), \text{ and} \tag{3}$$

4. The budget of the eddy available potential energy AE,

$$\frac{\partial AE}{\partial t}=CA-CE^*+\mathrm{BAL}(AE). \tag{4}$$

The B terms above represent the pressure interaction at the boundaries of an open system; the C terms represent the conversions or transfer of energy among various modes; and the BAL terms indicate the residual needed to balance equations (1) to (4). When equations (1) to (4) are broken down into their spectral components, two extra terms appear—$LK(n)$ and $LA(n)$. They are related to nonlinear redistribution of energy between waves—$LK(n)$ for the eddy kinetic energy and $LA(n)$ for the eddy available potential energy. The expansion of each term may be found in the appendix. The rather crude resolution in the vertical imposed a specific method of computation of the vertical motion. The vertical motion ω in the pressure coordinate system was obtained from the adiabatic-thermodynamic method

$$\omega=\frac{\partial T/\partial t+(g/f)\cdot J(z, T)}{\sigma}. \tag{5}$$

This equation was then transformed into the complex Fourier domain yielding a spectral component for each wave number n (Paulin 1968). The daily character of the data imposed a 48-hr centered time difference for the temperature tendency in equation (5). The stability factor $-\sigma$ was taken to be a function of pressure only. The magnitudes of this factor were based on a 5-day average (Jan. 12 to 16, 1959) previously computed by Paulin (1968). They closely agreed with those computed by Gates (1961) for the January average. All the terms other than CE^*, CZ^*, BGE, BGZ which include a correlation of ω with some other variable have been deleted. They are on the whole much smaller in magnitude and will not affect the results significantly (Paulin 1968). The $LK(n)$ and $LA(n)$ terms are expanded in the appendix. It can be noted that in this case the terms containing the correlation of the vertical motion with the horizontal motion have been deleted in the expansion. These terms are, on the whole, small; and their deletion does not affect the results significantly except maybe locally in some special circumstances, as shown by Paulin (1968).

It is to be noted that because of the character of our vertical motion computational method as shown in equation (5), the computed CZ^* and CE^* will not give a true representation of the exchanges between available potential energy to kinetic energy. The computed energy conversions give a mixture of the true conversions and the

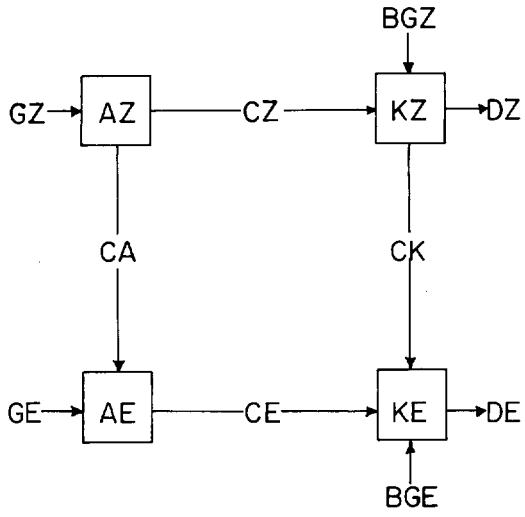

FIGURE 1.—Energy flow diagram showing the positive direction in conversions, generations, and dissipation.

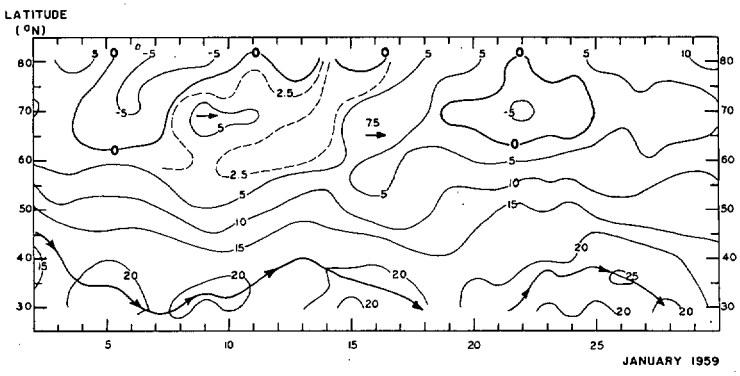

FIGURE 2.—Isopleths of the mean zonal wind (m sec^{-1}) at 500 mb as a function of latitude. The dark continuous line represents the locus of the wind maxima during the month.

added effect of radiative available potential energy generation (Holopainen 1963, Wiin-Nielsen 1964, Muench 1965). The relationships between the computed conversions CZ^*, CE^*, the true conversions CZ, CE, and the generation terms GZ and GE are

$$CE^*=CE-GE \tag{6}$$

and

$$CZ^*=CZ-GZ. \tag{7}$$

A few words of caution are also necessary with respect to the BGZ and BGE terms as applied to our system. These terms represent the effect of the work done by the pressure forces at the horizontal boundaries of our chosen volume. The pressure forces across the vertical boundaries are deleted as relatively insignificant. We have divided our vertical section of interest into two layers—100 to 25 mb and 25 to 0 mb.

The sign convention used for the energy conversion terms is given in the schematic energy flow diagram of figure 1. The direction of the arrows indicates positive transfer.

4. SYNOPTIC EVENTS OF JANUARY 1959

The tropospheric weather pattern of January 1959 may be described as very stable and persistent. A pulsating blocking regime controlled the month's circulation in the troposphere. The oscillation in the amplitude of the block was found to have a period of 10 to 12 days in the mid-latitudes. Figure 2 describes the latitudinal and time distribution of the zonal winds at 500 mb. Minima in the average zonal flow regime are found from the 7th to 9th, the 16th to 19th, and near the end of the month. The sequence of events related to the stratosphere has been given by Boville et al. (1961), Steiner (1961), and Godson and Wilson (1963) using the 25-mb information. Their results are summarized next. The end of December 1958 presented a circumpolar vortex with minimum temperature below −80°C and a contrasting maximum temperature of −45°C near Japan. By the 3d of January, three large troughs appeared, one over North America and the others over western Europe and eastern Asia. Gradually, an extensive high-pressure area strengthened to cover the whole of the North Pacific as the −45°C isotherm spread from the area north of Japan to the whole of Kamchatka. The warming advanced gradually eastward over North America from the 8th to the 18th, preceded by a deepening cold trough that reached the east coast of North America by the 18th. During the same period, the eccentricity of the flow increased as the center of polar vortex shifted toward Europe. From the 18th to the end of the month, the polar vortex retrogressed over the Canadian Archipelago, with a very specific organization in the contour structure. The strong warm High that had covered the North Pacific and western Canada on the 18th collapsed as the North American trough retrogressed to a line from central Canada to the midwestern United States by the end of the month. The trough over western Europe collapsed while the trough over eastern Siberia strengthened somewhat. Visually, the 25-mb flow pattern was remarkably bipolar with very little eccentricity by the end of the month.

5. TWENTY-FIVE-MILLIBAR ENERGETICS

This section will present the energy modes, their tendencies, and the transfers relating them in order to find the direction in which energy flowed during January 1959. The daily variations of the energy modes are displayed in figure 3, and details on the daily energy conversions appear in table 1.

The zonal available potential energy AZ may be characterized by an oscillation with a 20-day period (fig. 3) having its minimum about the middle of the month. The eddy available potential energy AE has a similar 20-day oscillation but out of phase with AZ (fig. 3).

The time oscillations of the eddy kinetic energy KE have the largest amplitudes of the energy modes, and the four peaks occurring on the 3d, 13th, 17th, and 28th which are of special interest may be found in figure 3. The odd

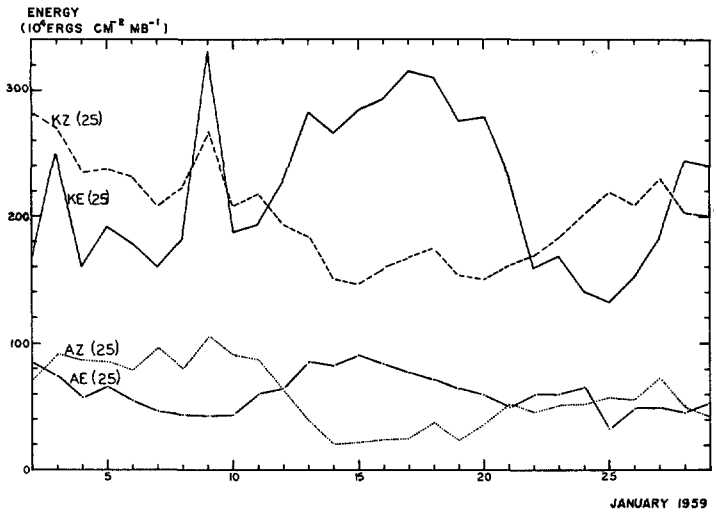

FIGURE 3.—Daily variations of the various energy modes at 25 mb.

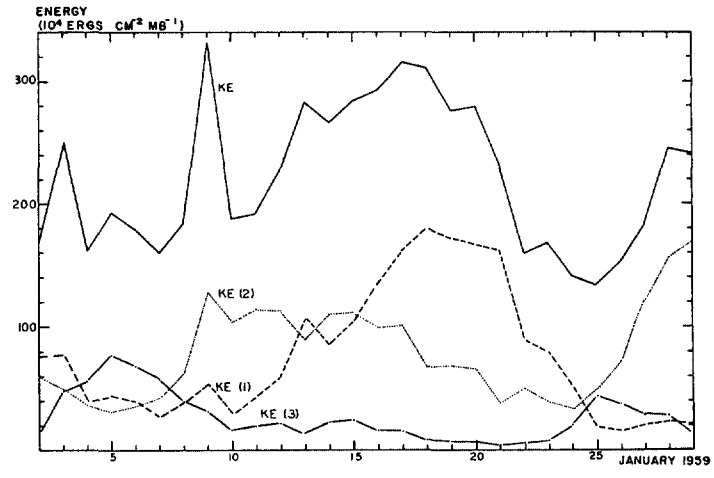

FIGURE 4.—Spectral partition of the eddy kinetic energy at 25 mb.

TABLE 1.—*Energy conversions at 25 mb during January 1959; units, ergs cm⁻² mb⁻¹ sec⁻¹*

Date	*CA*	*CE**	*BGE*	*CK*	*BGZ*	*CZ**
2	4.20	4.80	13.20	−1.40	−16.78	−6.67
3	2.99	4.87	10.25	−1.22	−11.02	−4.87
4	2.60	3.72	8.57	.21	−5.59	−2.79
5	3.19	3.33	8.83	−1.01	−7.71	−3.59
6	2.80	4.72	10.05	−1.22	−8.92	−4.22
7	2.73	3.82	7.29	−1.30	−4.49	−2.58
8	4.03	4.72	7.99	.33	−9.95	−5.12
9	2.90	2.76	6.02	−2.35	−8.71	−3.93
10	7.07	6.57	14.25	−2.55	−6.46	−3.95
11	7.66	7.54	15.09	−3.74	−5.29	−3.17
12	6.89	6.21	16.62	−2.91	−5.12	−2.63
13	6.65	5.23	17.22	−.15	−1.51	−1.30
14	3.28	2.42	10.61	−3.10	−6.09	−2.38
15	3.21	3.33	10.39	−6.35	−12.38	−3.17
16	2.14	2.22	7.46	−7.20	−8.25	−2.36
17	2.29	3.34	8.94	−5.15	−8.98	−2.93
18	1.61	3.14	6.29	−2.62	−.50	−.16
19	2.09	2.82	12.69	−.77	−1.33	−.81
20	2.86	4.83	12.54	−1.14	−9.39	−3.93
21	2.14	5.03	16.37	.15	−6.08	−2.57
22	4.46	2.73	16.32	.09	−6.18	−3.08
23	5.17	4.68	13.14	−2.06	−6.34	−3.04
24	4.36	8.66	15.32	−1.51	−7.23	−3.95
25	2.62	4.27	7.96	.60	−4.64	−2.13
26	3.24	3.53	7.17	1.64	−6.29	−3.64
27	4.23	5.40	9.04	.06	−7.22	−3.17
28	3.85	4.63	9.07	−.41	−.11	−.73
29	2.15	2.68	7.08	−2.04	1.23	−.99
30	2.65	5.21	11.78	−6.20	−.95	−.00
Mean*	3.66	4.39	10.95	−1.84	−6.29	−2.89
Std. dev.	1.62	1.53	3.46	2.19	3.93	1.50
Conf.	.52	.49	1.11	.70	1.27	.48

*Results based on observations taken at 0000 GMT each day; mean, arithmetic mean for the month; std. dev., standard deviation; conf., 95-percent confidence range for the mean according to a Student's "t" test

peak on the 9th is not substantiated by the energy transformation terms. The peaks on the 3d and 13th may both be related with the eddy pressure interaction process *BGE*. The second peak also results from the baroclinic part of the *CE** process. The continuous but less rapid increase of *KE* from the 14th to the 17th is found to be due to both *BGE* and *CE* processes. The drop in *KE* after the 17th is difficult to explain, at least if one uses the *BGE* term valid for the 0- to 25-mb layer. However, the *BGE* term computed over the 100- to 25-mb layer (fig. 5) increases rapidly from the 16th to the 18th and declines sharply afterward. It is thought that the eddy geopotential flux, which is progressing upward, interacts with the 25-mb level temporarily and increases its eddy kinetic energy before the 17th and then is transmitted to the higher levels included in the 0- to 25-mb layer. The energy flow that led to the midmonth maximum in *KE* at 25 mb may be given schematically as

$$\begin{array}{c} AE \rightarrow KE \rightarrow KZ \\ \uparrow \\ \uparrow \\ \uparrow \\ BGE \end{array}$$

where the rates of transfer are roughly proportional to the number of arrowheads. In a similar fashion, the energy flow

$$\begin{array}{c} AE \rightarrow KE \leftarrow KZ \\ \uparrow \\ \uparrow \\ BGE \end{array}$$

leading to the last maximum in *KE* on the 28th is somewhat similar, except that *CK* is now positive and small.

It is instructive to examine the horizontal scales involved in the 25-mb fluctuations of *KE*. The behavior of the three higher amplitude spectral components of *KE* at wave numbers 1, 2, and 3 is given in figure 4. A strong wave number 1 pattern, or eccentric pattern, explains well the midmonth (17th) maximum, and the peaks on the 9th and 28th are due to a bipolar or wave number 2 pattern. A minor maximum at the scale of wave number 3 about the 5th is concurrent to minima in waves 1 and 2. Nonlinear wave interactions between these waves are indicated during the following 5 days. This spectral analysis is equivalent to the 25-mb synoptic description given earlier. The wave number 3 pattern reflects the existence of the three main troughs found early during the month. By midmonth, a strong eccentric system had formed as a warm wave progressed over North America and the polar

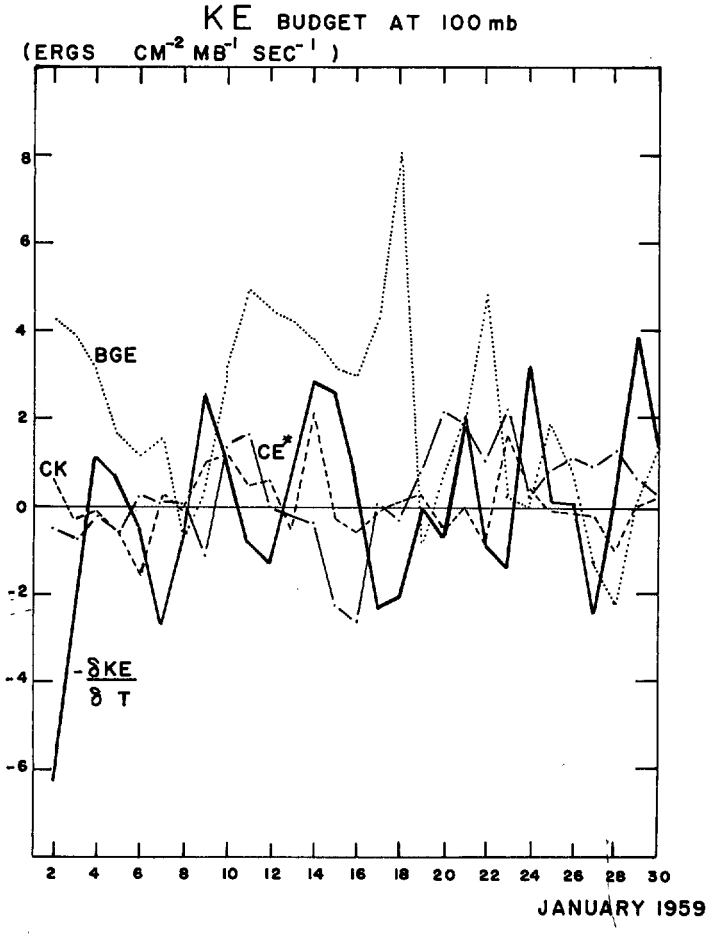

FIGURE 5.—Budget of the eddy kinetic energy *KE* at 100 mb.

vortex shifted toward Europe. By the end of the month, the flow became bipolar as the polar vortex had retrogressed over the Canadian Archipelago. The midmonth warm High found over the Pacific and western Canada collapsed gradually with the change in the circulation pattern by the end of the month. In a gross fashion, the net changes in total eddy kinetic energy at 25 mb may be explained satisfactorily by the spectral components *KE*(1), *KE*(2), and *KE*(3). Further, the individual components are found to have periods of about 20 days, as shown in figure 4.

A negative time correlation is found to exist between the zonal kinetic energy *KZ* and the eddy kinetic energy *KE* at 25 mb (fig. 3). The reversal in the *KZ* and *KE* trends in time are reflected in the daily intensities of the barotropic transfer *CK* in table 1. It is to be noted that contrary to its eddy counterpart, *BGE*, the zonal pressure interaction *BGZ* is negative throughout the month, except maybe on the 29th. *CZ** and *BGZ* fluctuate simultaneously in time. Some coherence is then indicated between these two processes.

6. ONE HUNDRED-MILLIBAR ENERGETICS

The magnitudes of the energy conversions at 100 mb are about half those at 25 mb. Characteristically, most conversions change sign frequently, making the choice

TABLE 2.—*Types of baroclinically active energy cycles during January 1959 (as defined in the text) at 25 and 100 mb and eddy (total and spectral) pressure interaction on the 25- to 100-mb layer occurring with peaks in the eddy kinetic energy at both 25- and 100-mb levels; units of the pressure interaction terms, ergs cm^{-2} mb^{-1} sec^{-1}*

Date of peaks	8-9	13	17	20	23	28
25-mb cycle type	1	1	1	1	1	1
100-mb cycle type	1	1	1	1	2	1
BGE	−.21	4.22	4.27	.65	.20	−2.26
BGE(1)	−1.10	2.48	2.83	2.92	1.81	−1.30
BGE(2)	1.78	1.36	1.01	−.55	.75	.02
BGE(3)	−.47	.64	−.07	−1.72	−.62	−.34

of a characteristic energy flow more difficult. Two baroclinically active types of energy flows associated with maxima in the eddy kinetic energy mode at 100 mb have been isolated:

Type 1.

$$AZ \rightarrow AE \rightarrow KE \rightarrow KZ$$
$$\updownarrow$$
$$BGE$$

and

Type 2.

$$AZ \rightarrow AE \rightarrow KE \leftarrow KZ.$$
$$\updownarrow$$
$$BGE$$

The energetics at 100 mb are compared with those at 25 mb in table 2. The days with local maxima in *KE* at either or both 25 and 100 mb are selected. The corresponding energy flow type is given at each level. The direction of energy flow due to the *BGE* mechanism (total eddy and spectral) as applicable to the 100- to 25-mb layer is also given. The following remarks may be inferred from table 2. All peaks in eddy kinetic energy are associated with active energy cycles. The peaks on the 13th and 17th appear together with maxima in the transmitted energy from the troposphere (see also fig. 5) by the *BGE* mechanism. Further, the pressure interaction at wave number 1, *BGE*(1), is more active than its wave number 2 counterpart, *BGE*(2). The dominance of *BGE*(1) over *BGE*(2) about the middle of the month is reflected in the eccentric structure of the circulation at 25 mb, already noted in the synoptic discussion and clearly shown earlier in figure 4. A similar spectral structure characterizes the 100-mb circulation. *KE*(1) is larger than *KE*(2) from the 18th to the 25th, and *BGE*(1) is more active than *BGE*(2) from the 12th to the 23d, except on the 19th when *BGE*(1) is strikingly negative (−1.61 ergs cm^{-2} mb^{-1} sec^{-1}). The transitory peak of *KE* at 100 mb on the 28th must be due to a strong flux of this energy from the southern boundary since all other transfer processes contribute to a decrease in this mode at this level. It is concluded that both eccentricity and bipolarity of the lower stratospheric flow were on the average transmitted from below during January 1959 and that the period of more intense and lasting eddy kinetic energy past the middle of the month was caused mainly by the spectral pressure interactions *BGE*(1) and *BGE*(2), with the former being more effective than the latter.

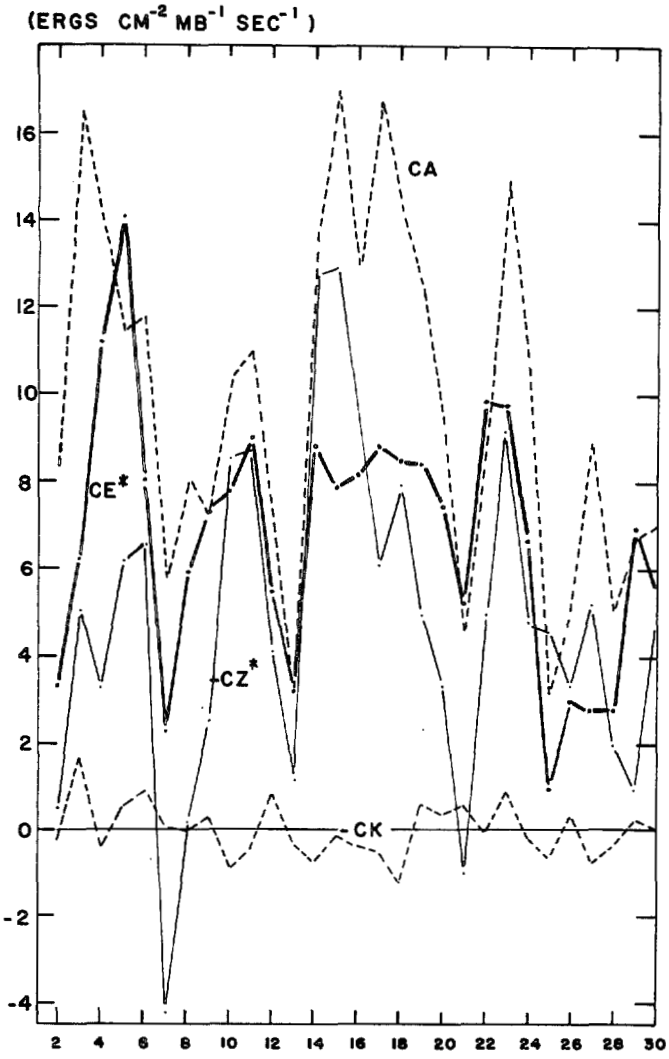

FIGURE 6.—Energy conversions at 500 mb during January 1959.

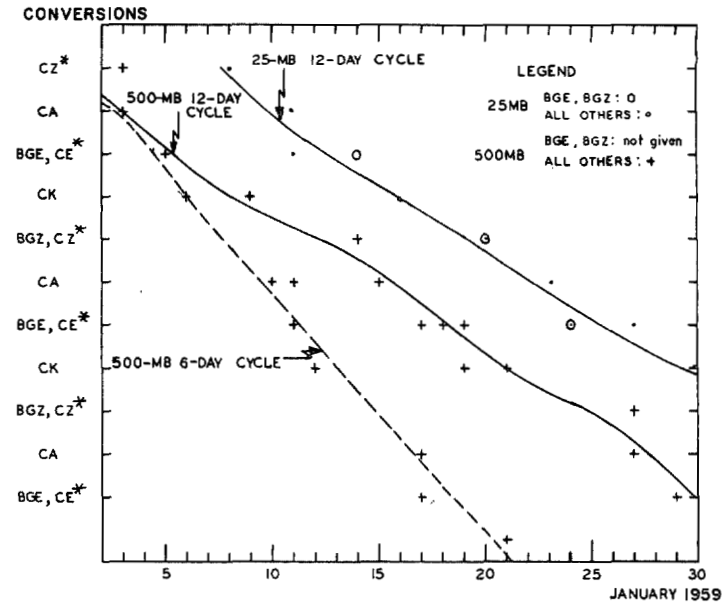

FIGURE 7.—Time loci of energy conversion maxima at 25 and 500 mb.

7. FIVE HUNDRED-MILLIBAR ENERGETICS

The energy flow at 500 mb follows either active type 1 or 2. Figure 6 illustrates the daily variations of the four transfers *CA*, *CE**, *CK*, and *CZ**. The 500-mb energetics may be characterized by about five large amplitude pulsations in *CA*, *CE**, and *CZ**, also shared in a lesser fashion by *CK*. These pulsations occur about the 4th, 11th, 16th, 22d, and 27th, averaging a 5- to 6-day period. A subharmonic may be inferred from the time lapse of 10 to 12 days separating the peaks with largest amplitude. A comparative diagram relating energetic events at 500 and 25 mb is presented in figure 7. Maxima in individual energy conversions are plotted in time at both 25- and 500-mb levels. The energy conversion terms are given in the ordinate following the order in which they appear in a normal energy flow of a baroclinic troposphere. The plot of these conversion maxima at some level will characterize the period of their time fluctuations. The 500-mb locus (broken curve) exhibits a time oscillation with a 5- to 6-day period. The 25-mb locus (upper continuous curve) reveals the existence of a time oscillation with a 10- to 12-day period. Furthermore, when the strongest 500-mb maxima are plotted in time (lower continuous curve), a sub-harmonic of the basic time series appears with half the basic frequency, that is, recurring every 10 to 12 days. The 25-mb locus lags the 500-mb 12-day period locus by about 8 days. The time difference between the two loci appears to be a minimum about mid-January (lag of about 6 to 7 days). After assuming that the 25-mb fluctuations are associated with the energy transmitted from 500 mb, a time lapse for upward progression of 5 to 7 days agrees with theoretical results (Charney 1949, Charney and Drazin 1961, Rutherford 1969) and some observational results (Muench 1965).

One recalls the persistent blocking pattern that characterized the 500-mb circulation during January 1959. Some pulsations were observed in the strength of the block. The strongest blocks occurred on the 6th to 9th, 15th to 19th, and near the end of the month—all three blocks have characteristic maxima in *CA* and *CE**. *CK* is also mainly positive (*KZ*→*KE*). The strength of the midmonth block can be found from the large values of *KE* and *AE* (not shown) at 500 mb. It is therefore concluded that blocking circulations are produced by an energy flow of the type

$$AZ \rightarrow AE \rightarrow KE \leftarrow KZ.$$

The strength of the block is proportional to the individual energy conversion magnitudes and durations. Furthermore, part of the energy associated with the three blocks of January 1959 (6 to 9, 15 to 19, and 25 to 28) are found to have propagated upward, as evidenced by maxima in eddy kinetic energy at 25 mb that are observed slightly later (9th, 17th to 20th, and 28th to 30th).

In summary, during January 1959, the 500-mb circulation resulted from the energy flow

$$AZ \rightarrow AE \rightarrow KE \leftarrow\rightarrow KZ.$$

It has been found that the transfer *KZ*→*KE*, when

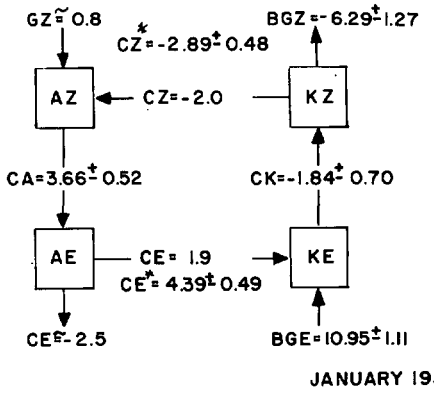

FIGURE 8.—Monthly mean energy conversions at 25 mb; units, ergs cm^{-2} mb^{-1} sec^{-1}.

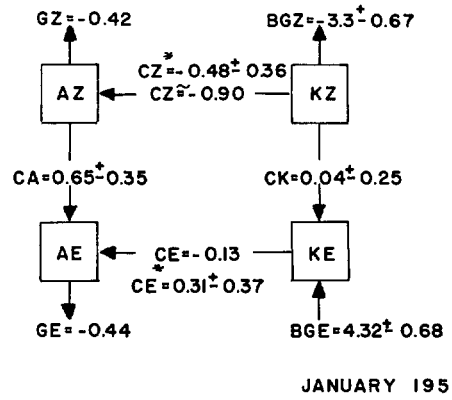

FIGURE 9.—Monthly mean energy conversions at 100 mb; units, ergs cm^{-2} mb^{-1} sec^{-1}.

coupled with maxima in positive *CA* and *CE** conversions, led to blocking patterns whose importance was proportional to the intensity and persistence of the above-mentioned energy transfers. Furthermore, a 10- to 12-day cycle in the energy conversions was found in both the troposphere and the stratosphere, the cycle at 500 mb leading the one at 25 mb by about 8 days. The 500-mb 12-day period was mixed with a second cycle of twice this frequency. Their influence reached the 25-mb level a few days later through the vertical propagation of the eddy geopotential flux.

8. MONTHLY MEAN ENERGETICS

The monthly mean energy flows at 25, 100, and 500 mb are presented in figures 8, 9, and 10, respectively. The intensities of the transfers are given with the 95 percent confidence range for the mean using a t-test, assuming that the 29-day data are independent. Some new conversion symbols appear on the graphs. *GE* and *GZ* stand for the eddy and zonal generations of available potential energy, respectively. Some representative values (Paulin 1968, 1969) are chosen for these processes. *CE* and *CZ* are obtained from the computed *CE** and *CZ** once *GE* and *GZ* are chosen.

The 25-mb energy transfers (fig. 8) follow the well-known energy cycle of a baroclinic troposphere with the added significant pressure interaction mechanism—*BGE* and *BGZ*. The *BGE* process provided the main source of eddy kinetic energy. It was postulated that the eddy frictional dissipation *DE* and the flux of *KE* across the lateral boundaries provided the required sink. The zonal and eddy generations of available potential energy at 25 mb were taken to be 0.8 and −2.5 ergs cm^{-2} mb^{-1} sec^{-1}, respectively. This choice was based on the results of Perry (1966) and Paulin (1969).

The energy flow at 100 mb averaged over the month (fig. 9) may be characterized by the small statistical significance in the average direction of the transfers at the 95-percent confidence level. Computed values of *GZ* (0.42 erg cm^{-2} mb^{-1} sec^{-1}) and *GE* (−0.44 erg cm^{-2} mb^{-1} sec^{-1}) for a 5-day period in January 1959 were taken from Paulin (1968). *BGE* and *BGZ* are computed over the 100- to 25-mb layer. The 100-mb level is baroclinically passive

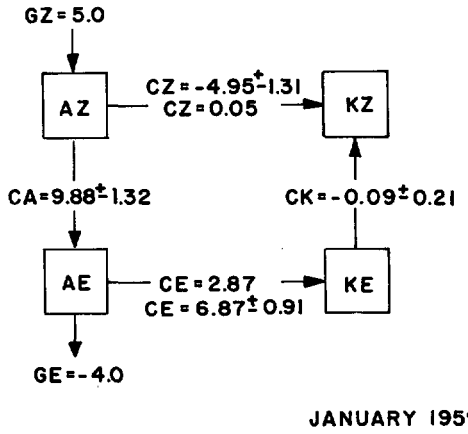

FIGURE 10.—Monthly mean energy conversions at 500 mb; units, ergs cm^{-2} mb^{-1} sec^{-1}.

on the average as cold air is rising and warm air subsiding in the zonal plane, that is, *CE* is negative.

The 500-mb level exhibits the normal energy cycle found in a baroclinic atmosphere (fig. 10). Moderate baroclinic exchanges result after a chosen *GE* generation of −4 ergs cm^{-2} mb^{-1} sec^{-1} (Brown 1964, Krueger et al. 1965, Vernekar 1967) is taken from the computed *CE**. Although the barotropic exchange *CK* is in the normal direction of the average (*KE*→*KZ*), the sign is not significant in our confidence range for the mean. The strength of the *CA* mechanism supports a very effective eddy heat transport northward, on the average. This reflects the persistence of the blocking regime during the month. A value of 5 ergs cm^{-2} mb^{-1} sec^{-1} was taken for *GZ*. It agrees with the values computed by various investigations (Brown 1964, Perry 1966, Paulin 1968). The chosen generation *GZ* is counterbalanced by the loss of available energy in its eddy form at a rate of 4.0 ergs cm^{-2} mb^{-1} sec^{-1} through the chosen *GE* value. A large imbalance in the *AZ* and *AE* modes may be partially explained by the use of an adiabatic vertical motion model at 500 mb. The *GE* and *GZ* rates chosen are strictly applicable to the troposphere and are not fully representative of the situation at the 500-mb level. The concept of available potential energy applied to an open volume may lead to further inaccuracy.

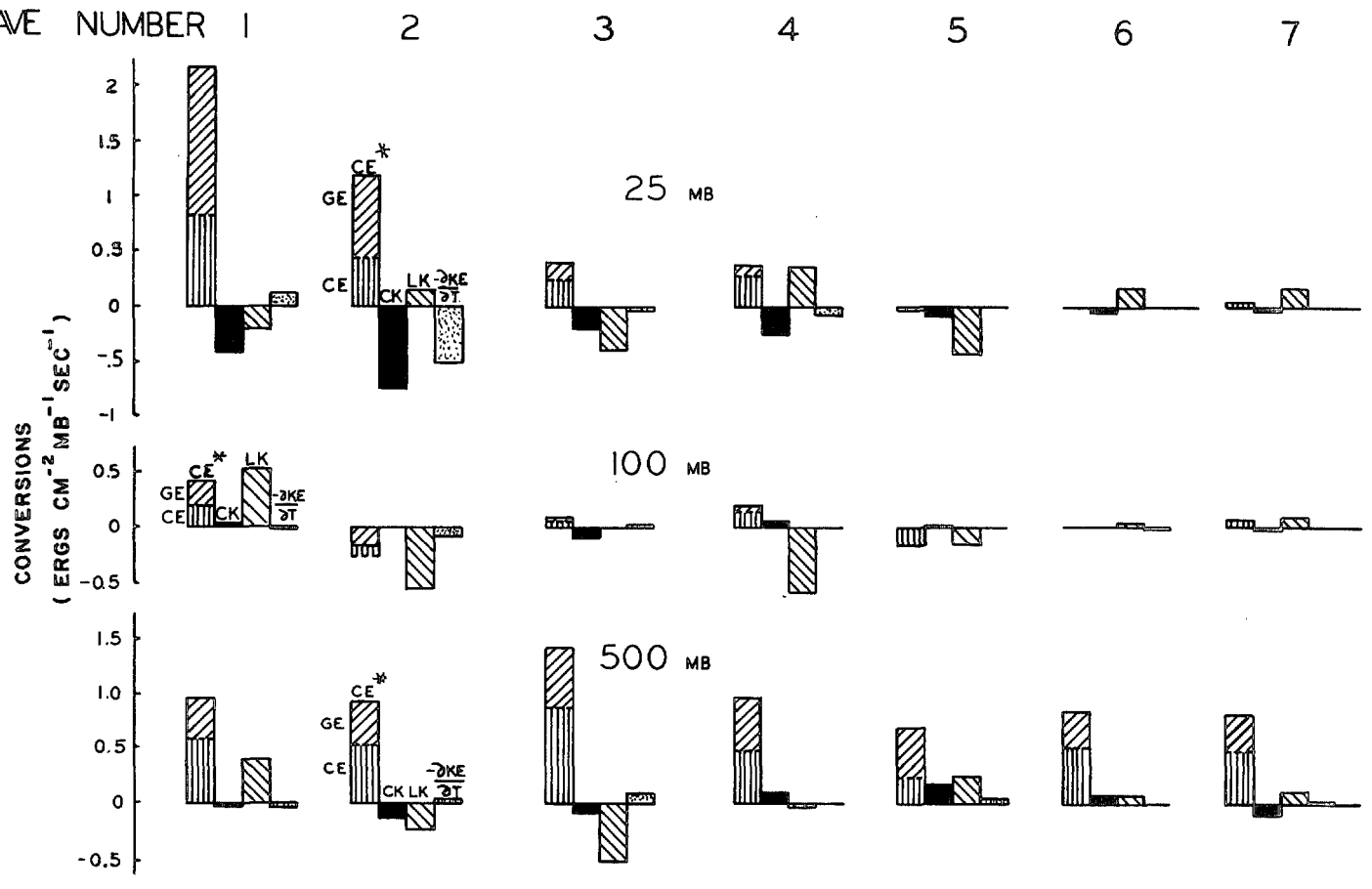

FIGURE 11.—Monthly mean spectral kinetic energy budget for January 1959.

The rate at which eddy kinetic energy is being lost by upward propagation while the rate at which zonal kinetic energy is being gained is shown in figure 14 to be -2.5 and 0.15 ergs cm^{-2} mb^{-1} sec^{-1}, respectively. These computed BGZ and BGE processes were found by Paulin (1968) and are applicable to the 200- to 300-mb layer during 5 days in mid-January 1959.

9. SPECTRAL KINETIC ENERGY

The present section deals with the mean monthly results pertaining to the spectral distribution of the kinetic energy at 25, 100, and 500 mb. Figure 11 displays the significant energy processes.

At 25 mb, the spectral energy flows are clearly dominated by processes at the scale of wave numbers 1 and 2, followed by those of wave numbers 3 and 4. The $CE(n)$s were recovered from the computed $CE(n)$*s using the values of $GE(n)$ computed by Paulin (1968) and valid during mid-January 1959. The budgets of $KE(1)$, $KE(2)$, and $KE(3)$ are acceptable if one assumes that the frictional effects counteract the pressure interaction mechanism. The spectral baroclinic process $CE(n)$ is found to decrease with scale. On the other hand, the barotropic $CK(n)$ process disperses energy into the zonal flow with wave number 2 energy being most efficiently transferred. The nonlinear wave interaction process $LK(n)$ disperses the wave energy in such a way that adjacent wave numbers are mutually connected—wave numbers 1, 3, and 5 feed 4 and 2 with wave number 4 being favored.

The 100-mb spectral kinetic energy budget is again characterized by weak transfer rates. The $CE(n)$ magnitudes have been obtained using previously computed $GE(n)$ values from Paulin (1969). In any case, most conversions are small, and the only statistically significant conversion (weakly significant) belongs to the nonlinear wave interaction $LK(n)$. Figure 11 shows that wave number 1 kinetic energy is maintained mainly by exchanges from wave numbers 2 and 4.

Brown (1964) has computed the spectral generation of available potential energy in the troposphere for January 1959. His results were integrated graphically to yield generations applicable between 30° N. and 80° N. Our implied $CE(n)$ baroclinic process was maximum at the scale of wave number 3 and minimum at wave number 5; the other scales portrayed at 500 mb are about evenly baroclinically active. The 500-mb nonlinear wave interaction feeds $KE(1)$ and $KE(5)$ at the expense $KE(3)$ mostly and $KE(2)$. Fair balances would result in the spectral budgets if losses through frictional dissipation and pressure interaction canceled each other.

It has been found so far that at 25 mb, in the monthly average, the changes in eddy kinetic energy were mostly explained by the flow at the scale of wave numbers 1, 2, and to a lesser extent, 3. It is interesting to visualize qualitatively the effect of the nonlinear interaction processes on the daily changes of the spectral kinetic energy

TABLE 3.—*Spectral eddy kinetic energy tendency $\partial KE(n)/\partial t$ and nonlinear wave interaction $LK(n)$ for wave numbers 1, 2, and 3 at 25 mb during January 1959; units, ergs cm^{-2} mb^{-1} sec^{-1}*

Date	$\frac{\partial KE(1)}{\partial t}$	$LK(1)$	$\frac{\partial KE(2)}{\partial t}$	$LK(2)$	$\frac{\partial KE(3)}{\partial t}$	$LK(3)$
2	−0.66	−2.08	0.90	1.49	2.96	0.71
3	−1.27	−1.02	−.06	−.18	2.37	−1.15
4	−1.10	−1.92	−.99	.51	1.30	.85
5	−.21	−1.29	−.56	.86	.50	.54
6	−.24	.77	.08	.45	−1.23	−1.50
7	.50	−1.05	1.28	1.59	−1.02	−1.48
8	.83	1.15	2.74	.65	−.79	.07
9	−.05	1.13	1.38	.28	−1.00	.30
10	−.21	1.06	−.60	−.08	−.62	.64
11	.42	.92	−.12	−.96	−.12	−.24
12	1.39	.64	−.72	−.17	.13	.00
13	.36	−.53	.13	1.14	−.08	−.65
14	−.06	−2.13	.13	−2.14	−.10	1.28
15	1.23	−2.00	−.88	−2.27	−.41	.31
16	1.12	1.40	−.62	−3.81	−.42	.94
17	1.41	.69	−.86	−3.84	.20	1.02
18	.95	1.75	−.25	.59	.28	−1.75
19	.45	1.93	.18	−2.38	.21	−.41
20	.69	−2.03	−.30	.05	−.40	−.52
21	−2.05	−2.38	−.25	1.27	−.88	−.12
22	−2.32	−.68	−.38	.05	−.20	−.74
23	−.38	−.58	−1.12	1.42	.62	−.68
24	−1.45	.14	.12	−1.36	.62	.50
25	−1.12	−1.31	1.35	.91	.92	−1.09
26	.00	−.61	2.32	2.12	−.16	−.84
27	.31	.34	1.75	.40	−.70	−1.30
28	.12	2.33	.86	1.27	−.18	−1.11
29	.15	1.61	.95	−1.19	−.45	−1.07
30	.29	2.65	.83	−1.56	.04	−.54
Mean*		−.22		.16		−.41
Std. dev.		1.66		2.42		1.06
Conf.		.53		.78		.34

*See also table 1.

tendencies. Table 3 presents the daily variations of these two parameters for wave numbers 1, 2, and 3, respectively. Inspection of table 3 yields the following noteworthy points:

1. The changes in $KE(1)$ are highly correlated with $LK(1)$ up to the 27th where an equally large but negative $CE(1)$ process offsets the large positive $LK(1)$ effect.

2. The changes in $KE(2)$ are very well related to the $LK(2)$ term, except where the $CE(2)$ process becomes occasionally dominant.

3. The correlation between $\partial KE(3)/\partial t$ and $LK(3)$ was not as high as it was for the two larger scales. $CE(3)$ was found to be frequently the significant process modulating the changes in $KE(3)$.

10. SPECTRAL AVAILABLE POTENTIAL ENERGY

The monthly mean budget of the spectral available potential energy at 25, 100, and 500 mb can be seen in figure 12.

At 25 mb, waves 1 and 2 are shown to be the most significant scales in the budget of the spectral available potential energy. Scales of waves 3 and 4 show transfers that average about 25 percent of those of the first two waves. Transfers of scales shorter than that of wave number 4 are insignificant.

$AE(1)$ is maintained mainly by interactions from both the zonal and wave number 2 available energy, in that order. On the whole, it loses energy throughout the month by radiative and baroclinic processes.

The $AE(2)$ budget is very similar to $AE(1)$ except for an important difference—it transforms its energy into wave number 1 available potential energy by the nonlinear wave interaction process. Because this scale is less baroclinically active than wave number 1, it exhibits a slight net increase during the month. The actual values of $LA(n)$ at 25 mb are given in table 4.

At 100 mb, $CA(1)$, $LA(1)$, $LA(2)$, $LA(3)$, and $LA(4)$ are found to be the only typical transfers for the month. All the energy transfers about the 100-mb spectral available potential energy mode are diminutive mirror images of those at 25 mb, on the average. Again, the $LA(n)$ magnitudes may be found in table 4.

At 500 mb, zonal available energy is converted into waves 1, 4, 5, 6, and 7 at about a rate of 1 erg cm^{-2} mb^{-1} sec^{-1}, while more intense northward heat transport is shown at wave numbers 2 and 3 (1.5 and 2 ergs cm^{-2} mb^{-1} sec^{-1}, respectively). The available energy in wave number 2 and to a lesser extent in wave number 1 is transferred to the available potential energy of waves 5 and 6. The significance of the nonlinear transfer from wave 2 is confirmed by table 4 where the mean magnitude of $LA(2)$ is found to be −0.84 erg cm^{-2} mb^{-1} sec^{-1} and its confidence range extends to 0.40 erg cm^{-2} mb^{-1} sec^{-1}. Again, the $GE(n)$ values were those of Brown (1964) for the troposphere in January 1959. The $CE(n)$ terms are abstracted in the usual manner.

Interlevel comparisons give some further clues into processes having a vertical significance. January 1959 has been shown to be a month of large northward eddy heat transport at 25 and 100 mb, being limited to the scales of waves 1 and 2 at the upper level while being fairly well distributed to the scales of waves 1 to 7 at the lower level. At 25 mb, the significant baroclinic CE processes are occurring at waves 1, 2, and to a lesser extent, 3 and 4; while at 500 mb, the scales at which these processes occur are predominantly wave number 3 followed by 1, with a lower but significant part played by the scales of wave numbers 2, 4, 6, and 7, in about equal intensity. The next important item is the nonlinear wave number 2 interaction leading to a significant sink of $AE(2)$ energy at all levels. $LA(1)$ channels energy to $AE(1)$ in the stratosphere while it acts as a sink at 500 mb.

The daily spectral changes of the available energy modes will now be analyzed to clarify the main processes attached to the current events at 25 mb. The daily variations in the total eddy and spectral (wave numbers 1, 2, and 3) available potential energy have been plotted in figure 13. The diagram may be compared with figure 4, corresponding to the similar variations in the eddy kinetic energy mode. Note that the plotted scales for AE are four times those of KE since the eddy kinetic energy per millibar has characteristically a larger magnitude in the stratosphere, whereas the opposite is found to be true in the troposphere (Paulin 1968). The magnitudes of $AE(3)$ are found to be negligible during the month. $AE(1)$ is found to explain most of the changes in the total eddy mode, except after the 26th, when $AE(2)$ takes over, and

406-039 O - 70 - 2

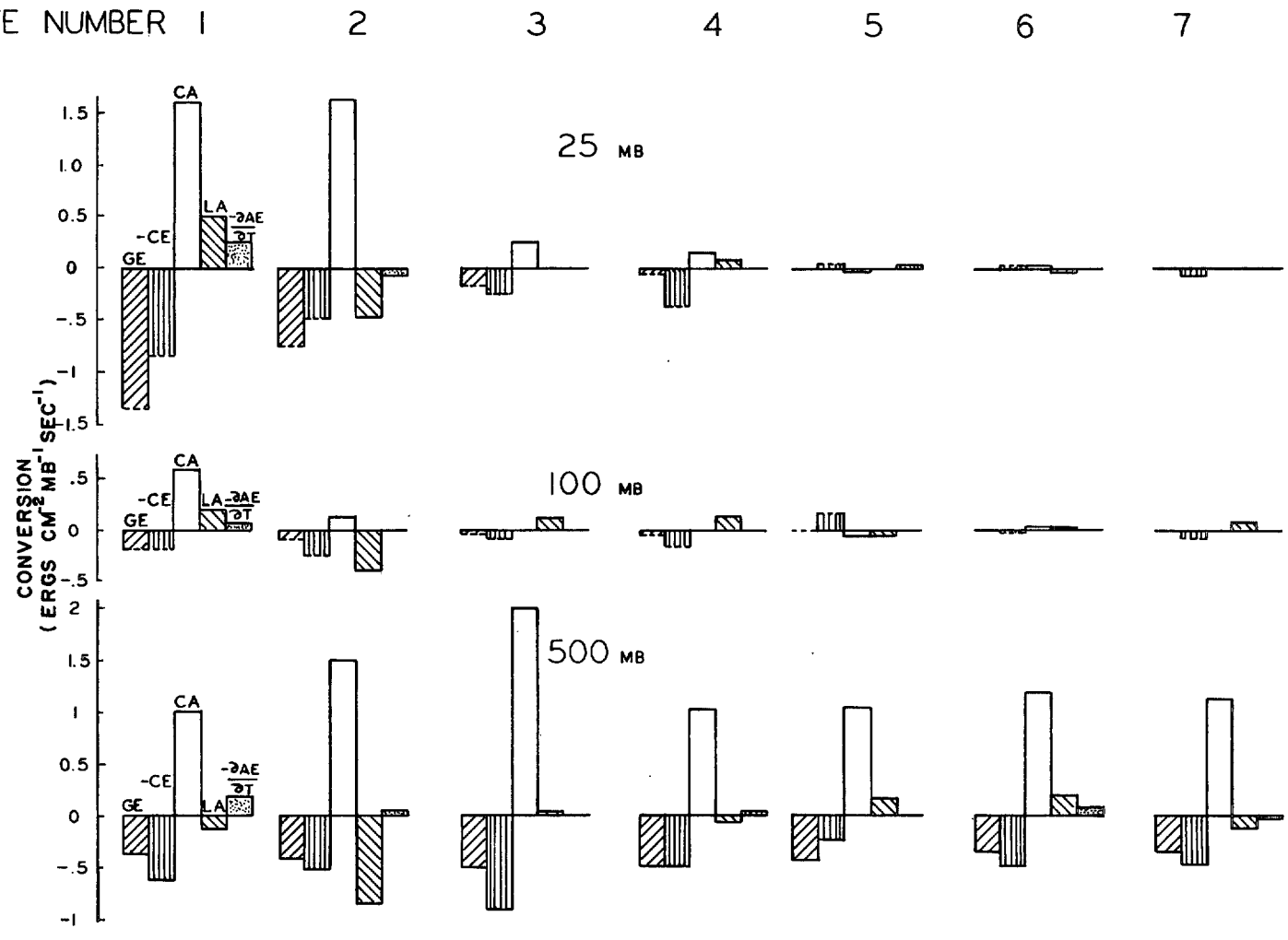

FIGURE 12.—Monthly mean spectral available potential energy for January 1959.

TABLE 4.—*Mean January 1959 nonlinear wave interaction term LA(n) for wave numbers 1 to 7 at 25, 100, and 500 mb and their associated standard deviation and 95-percent confidence ranges for the mean; mean units, ergs cm⁻² mb⁻¹ sec⁻¹*

LA(n)	25 mb			100 mb			500 mb		
Wave no. *n*	Mean	Std. dev.	Conf.	Mean	Std. dev.	Conf.	Mean	Std. dev.	Conf.
1	0.52	0.36	0.12	0.18	0.48	0.16	−0.07	1.09	0.35
2	−.48	.34	.11	−.34	.50	.16	−.84	1.25	.40
3	.00	.28	.09	.13	.36	.12	.02	1.84	.59
4	.10	.16	.05	.14	.36	.12	−.06	1.04	.33
5	−.01	.12	.04	.06	.40	.13	.16	.85	.27
6	−.02	.14	.04	.02	.45	.15	.21	1.27	.41
7	.01	.06	.02	.05	.35	.11	−.13	.50	.16

also from the 10th to the 13th when $AE(2)$ reaches almost the magnitude of $AE(1)$.

The daily changes in $AE(1)$ and $AE(2)$ may be found in figure 13, and the energy conversion values contributing to these changes are listed in table 5. The persistent increase of $AE(1)$ up to the 18th (fig. 13) is found to be caused by both $LA(1)$ and $CA(1)$. Together, they overcompensate the effect of the mixed radiative-baroclinic exchange $CE^*(1)$. The net decrease of $AE(1)$ is mainly due to a large $CE^*(1)$ conversion and later to a weakening and even change in sign of $CA(1)$. The general rise in $AE(2)$ up to the 10th (fig. 13) can be explained by the $CA(2)$ conversion that overshadows the effect of $CE^*(2)$. The decrease in $AE(2)$ afterward is due to low energy conversion activity at the scale of wave number 2. The net increase in $AE(2)$ by the end of the month is due to a stronger increase in $CA(2)$ than in $CE^*(2)$ and also in a reversal in $LA(2)$ that becomes positive in sign.

11. SUMMARY OF THE MONTHLY MEAN AND DAILY ENERGETICS

The results of this study are summarized by the mean January spectral flow diagram in figure 14. The 100-mb spectral conversions have been deleted since the amplitudes were rather small. At 25 mb, baroclinic activity is found in all the significant waves (1 to 4). Most conversions for $n \geq 5$ are weak and vary in sign. Wave number 1 is the dominant one in the baroclinic process followed by wave number 2. $CK(n)$ is negative for all values of n, leading to exchanges from the wave patterns to the zonal flow, with wave number 2 leading in importance. It is

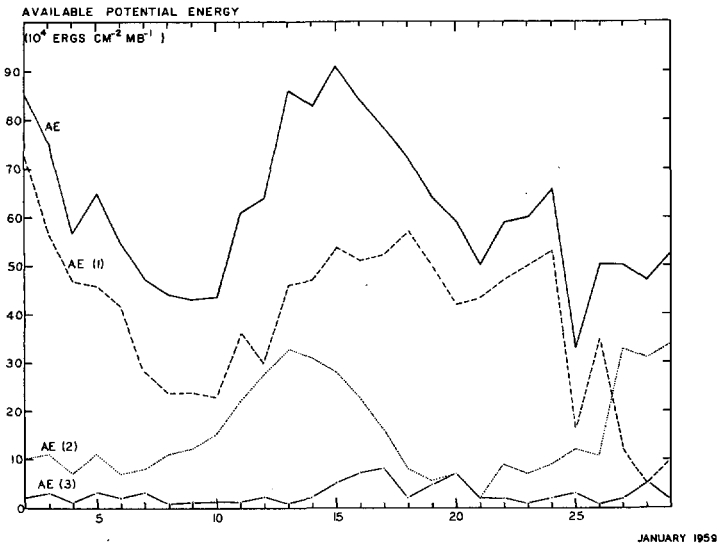

FIGURE 13.—Total eddy and spectral available potential energy for wave numbers 1, 2, and 3 at 25 mb.

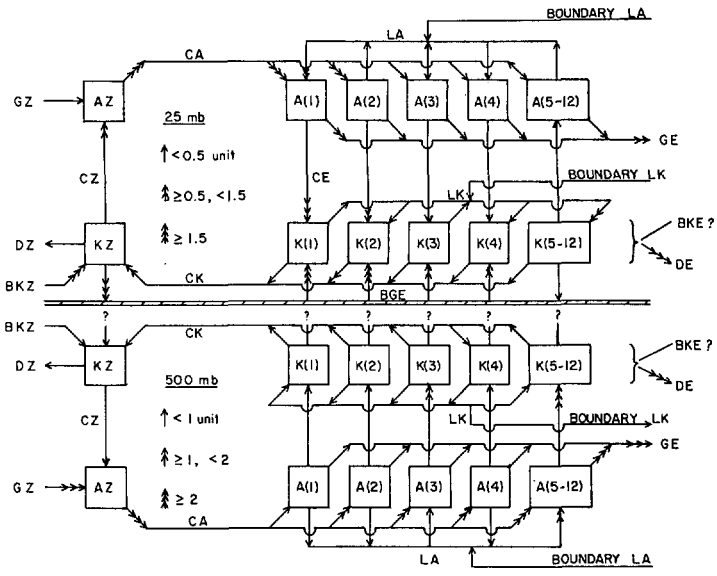

FIGURE 14.—Mean monthly spectral energy diagram at 25 and 500 mb for January 1959. The conversion intensities are proportional to the number of arrowheads as shown at the proper levels; units, ergs cm^{-2} mb^{-1} sec^{-1}.

TABLE 5.—*Spectral energy conversions CA(n), CE*(n), and LA(n) for wave numbers 1 and 2 at 25 mb during January 1959. The corresponding daily changes in AE(n) may be found in figure 13; units, ergs* cm^{-2} mb^{-1} sec^{-1}.

Date	*CA*(1)	*CE**(1)	*LA*(1)	*CA*(2)	*CE**(2)	*LA*(2)
2	2.50	2.80	0.35	1.60	1.50	−0.05
3	1.05	3.30	.60	.85	.70	−.10
4	2.75	2.80	.40	.20	.05	−.05
5	.80	1.35	.70	.60	−.50	−.45
6	1.10	2.75	.60	.65	.40	−.20
7	1.05	2.15	.35	1.70	1.70	−.05
8	1.75	1.00	−.35	1.70	1.35	−.15
9	2.05	2.10	.20	1.70	.60	−.40
10	2.30	.95	.50	3.95	3.80	−.45
11	2.95	2.30	.95	4.45	4.50	−.55
12	2.75	2.20	.55	3.55	2.65	−.70
13	2.60	1.50	1.40	3.35	2.95	−1.15
14	1.70	.70	.90	1.80	1.90	−.80
15	1.90	1.55	.95	.80	2.15	−1.05
16	1.45	1.05	.40	1.30	1.40	−.95
17	1.40	.35	.10	.75	1.90	−.45
18	1.30	1.80	−.15	.10	.80	.05
19	2.05	4.00	.75	−.15	−.95	−.80
20	3.10	4.40	.50	−.55	−.95	−.80
21	2.25	5.20	.35	−.30	−.95	−.45
22	4.75	3.55	.35	−.20	−1.20	−.80
23	3.60	3.65	.35	1.35	.80	−.25
24	2.80	8.70	.95	.75	−.95	−.85
25	.80	3.05	.75	.75	.25	−.45
26	−.15	1.55	.55	2.40	.80	−.60
27	−.70	1.50	.20	4.60	3.75	−.25
28	−.85	−.30	.15	3.90	4.70	.05
29	−.80	−1.10	.25	2.35	2.45	−.35
30	−.05	.40	.50	2.80	4.60	−.60

noted that although $KE(2)$ loses more to KZ than the other spectral kinetic energy modes, it nevertheless gains by the nonlinear exchanges, mostly from $KE(3)$ and $KE(5)$ followed by $KE(1)$. The general rise of cold air and subsidence of warm air in the meridional planes in conjunction with the zonal generation of available potential energy lead to a continuous increase of AZ at 25 mb. The zonal temperature field so produced is eventually deformed longitudinally by the local eddy air motion, which strongly pumps available energy into its eddy mode, especially in the scales of wave numbers 1 to 4, while the smaller scales play a minor role in the process. The $CA(n)$ transfers are large at waves 1 and 2 especially, their magnitudes amounting to five times those in wave numbers 3 and 4. The wave number 1 available potential energy mode is further increased by the redistribution between the temperature scales, most of the gain being at the expense of $AE(2)$. Because the longwave cooling is strongly negatively correlated with the temperature field, $GE(1)$ is negative and is the largest in absolute value among the spectral components of GE.

The 500-mb mean monthly spectral energy flow is also shown in figure 14. The diagram shows a typical tropospheric active energy flow. Some differences are noted, however. The $CK(n)$s are all very small, although in the direction usually observed in the troposphere. This can be traced back to the boundary problem at 30° N. Significant energy is flowing across this lateral boundary, and further processes are much more active at jet stream levels. The nonlinear kinetic wave interaction distribution does not agree with that of Saltzman and Teweles (1964) and Yang (1967, 1968), in whose studies wave number 2 and the cyclone waves were feeding both sides of the spectrum at 500 mb. Our results are closer to the Murakami and Tomatsu (1964) mean 1962 computations at 500 mb, in which wave numbers 2 through 6 fed the other waves and in which wave number 1 was receiving a large portion of the exchange. In the present study, wave numbers 2, 3, and 4 feed their kinetic energy to the other waves. The persistence of the $LK(1)$ process is being positive ($KE(1)$

gaining nonlinearly from other scales) has been found to be significant within the 95-percent range for the mean. At 500 mb, the monthly average spectral partition of the kinetic energy may be given in the following order of decreasing magnitudes: wave numbers 2 to 5 followed by 1, 6, and 7.

For summarizing the distribution in time of the stratospheric events among the various energy modes, a special spectral energy flow diagram for the 25-mb level is presented in figure 15. The relative significance of the transfers is indicated by the arrow. The significant "events" during the month are highlighted by the circle-in-square boxes, and the other sequential states of the energy reservoirs are circled only. Processes involving sources and sinks of energy have been labeled accordingly. The numbers in the circles specify the dates when the corresponding energy modes or transfers have significant intensity.

Three separate periods of high stratospheric eddy kinetic energy appeared during January 1959. The three periods appear to be causally related to blocking flows in the troposphere. The days of interaction from the troposphere to the stratosphere are January 7, 18 to 21, and 24 to 29. The time differences between the lower and upper events are somewhat variable because the upper events are not only associated with external energy but are also modulated by in situ processes such as the barotropic and baroclinic conversions, which may be intense enough to create a local time maximum in the eddy kinetic energy mode. The sequence of processes leading into the separate stratospheric events will be given in summary. The description of the various phases and exchanges may be best understood in relation to the flow chart on figure 15.

1. The rather sharp increase in $KE(2)$ from the 6th to the 9th is mainly due to simultaneous barotropic exchanges from the zonal, wave 1, and wave 3 kinetic energy modes, the baroclinic exchanges at this wavelength and time being rather small. The energy transferred to $KE(2)$ nonlinearly via $KE(3)$ originated in the troposphere through a pulse in the $BGE(3)$ term, while the other nonlinear interaction impact on $KE(2)$ from $KE(1)$ was through a moderate baroclinic exchange from $AE(1)$ by the $CE(1)$ process. $KE(2)$ declined through postulated dissipative effects from the 9th to the 10th and then rose again as a strengthening baroclinic exchange at the scale of wave number 2 coincided with a pulse in the pressure interaction mechanism $BGE(2)$. The net effect was that $KE(2)$ maintained its magnitude through to the 12th, leading to the first event. The bipolar pattern characterizing the first event had some degree of eccentricity as a local maximum of $AE(1)$ on the 11th and of $KE(1)$ on the 11th–12th period can be seen in figures 13 and 4, respectively.

2. The second event flows out of the first one. It is characterized by increasing eccentric activity in time, in response (a) to a rising wave number 1 pressure interaction acting on the 0- to 25-mb layer, in conjunction with the equivalent transfer at wave number 2 which peaks on the 15th concurrent with a nonlinear transfer from wave number 2 kinetic energy into wave 1, and (b) to moderate exchanges from $AE(1)$ fed nonlinearly by $AE(2)$. $AE(1)$ showed its peak on the 18th and then weakened as $KE(1)$ grew to its monthly maximum over the January 18 to 21 period. In summary, the second stratospheric event evolved from a large eccentricity in the flow pattern caused by three immediate mechanisms given in order of their intensity: (a) strong pressure interaction at the scale of wave number 1, originating from the troposphere, (b) a moderate nonlinear energy transfer from wave number 2, and (c) a moderate baroclinic transfer from $AE(1)$.

3. The third and last stratospheric event is characterized by the large bipolar flow found at the end of the month. The complex exchanges leading to this state from the highly eccentric state during January 18 to 21 are shown on figure 15. Only the significant processes will be sketched qualitatively here. The higher than average $KE(1)$ energy level led through a CK exchange to a KZ peak on the 18th and then an AZ peak on the 21st. An increase in the northward heat transport followed causing an $AE(1)$ maximum on the 24th simultaneous with a baroclinic exchange to $KE(1)$. A significant part of the $KE(1)$ energy is converted into the zonal mode, and KZ exhibits a maximum on the 25th. Possibly under the influence of both the temperature and vertical motion correlation CZ and the solar heating, the zonal available energy reached a local peak on the 27th. This set up strong northward heat transport at wave number 2 and a corresponding baroclinic transfer resulting in a large $KE(2)$ amplification. Two other processes are about equally significant, that is, the barotropic exchange from the zonal flow after the 27th and the pressure interaction $BGE(2)$ term which was likely associated with the blocking state found at the end of the month. A weaker process originating in the troposphere at wave number 3 converts energy into the 25-mb $KE(3)$ mode and then to $KE(2)$ nonlinearly, the mechanism explaining some part of the rise of $KE(2)$.

12. CONCLUSIONS

This study presents the daily and monthly mean energetics of January 1959. A rather coarse vertical resolution was used—height and temperature data at 500, 100, and 25 mb from 80° N. to 30° N. The energy modes and transfers pertaining to these three levels have been computed. These energy parameters have also been broken down to their spectral (Fourier) components. Interlevels and time dependences between these parameters have been inferred.

The average energy flow at both 25 and 500 mb was of an active baroclinic type. The 100-mb energy flow was characteristically of smaller amplitude and oscillated between a baroclinically passive and active type.

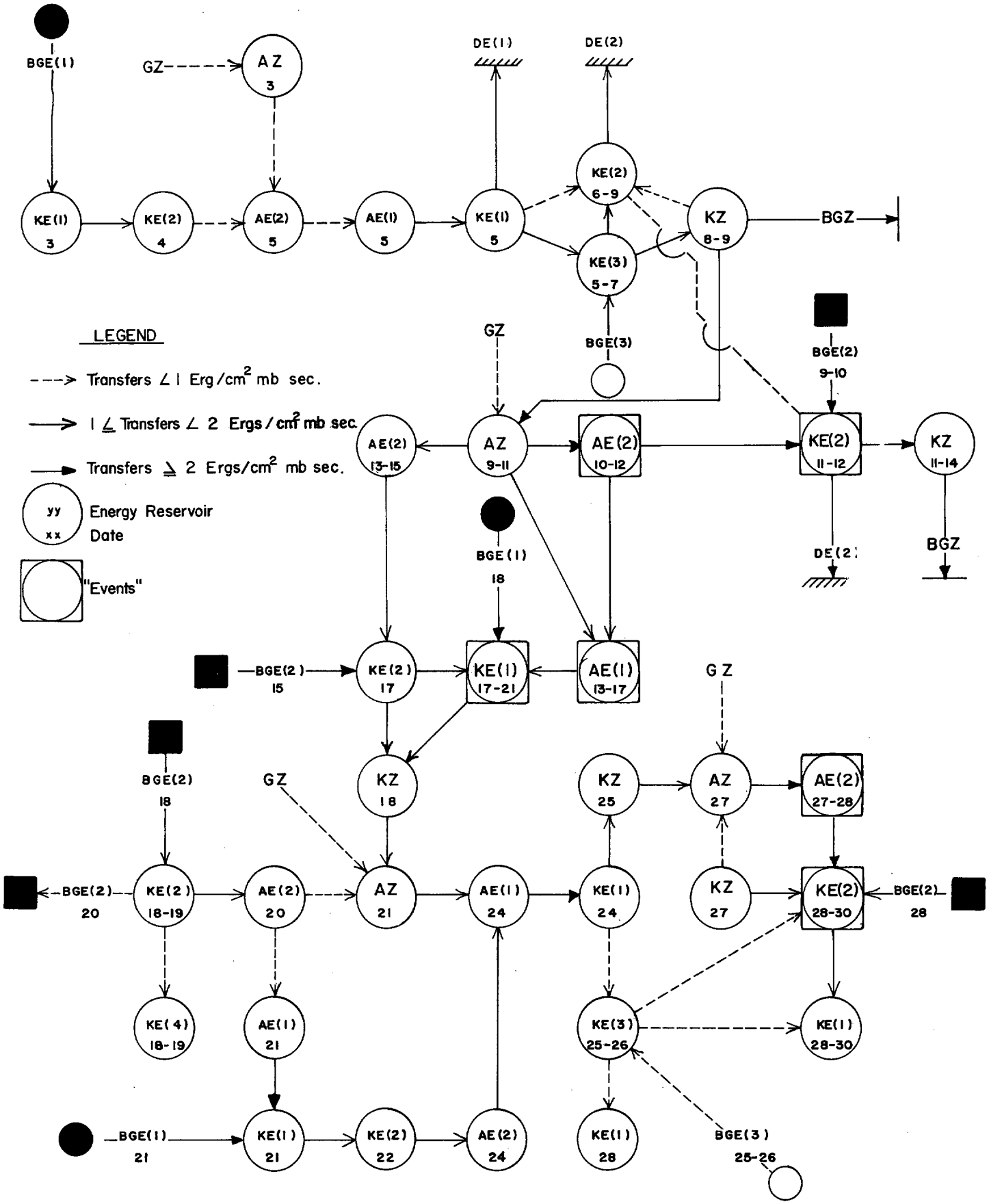

FIGURE 15.—Daily spectral energy conversions at 25 mb during January 1959; units, ergs cm^{-2} mb^{-1} sec^{-1}.

The eddy energy, kinetic and available potential, showed the scales of wave numbers 1 and 2 to be dominant, on the average, in the stratosphere (25 and 100 mb). At 500 mb, the emphasis was shifted to wave numbers 2 and 3. The planetary scale dominance over the synoptic scale at 500 mb is a manifestation of the stability and persistence of the blocking circulation found during January 1959. This larger scale dominance at 500 mb was also found in the eddy transfers $CA(n)$ and $CE^*(n)$.

The study found that the large-scale tropospheric blocking circulation in existence during January 1959 had a direct influence on the stratospheric eddy kinetic energy. The connecting link between the two layers has been found to be the upward progression and, later, partial absorption of planetary wave energy in the stratosphere. A 10- to 12-day fluctuation in the block was found to be followed by a pulsation of similar frequency in the eddy kinetic energy at 25 mb. Of the three pulses in the tropospheric block, the second one had the largest amplitude and was followed by a stratospheric warming at 25 mb. The contour pattern during the mid-January warming was eccentric in character; whereas on the other two occasions, the kinetic energy maxima at 25 mb were bipolar. In situ large-scale baroclinic processes contributed significantly to the occurrence and maintenance of the spectral kinetic energy maxima. Nonnegligible control of the large-scale kinetic energy mode was provided by the nonlinear wave energy transfers.

APPENDIX

The expansion of the various terms used in equations (1) to (5) are given here in their simplified forms. The symbolism used is defined at the beginning of the paper. The terminology follows that of Saltzman (1957).

$$\Phi_{fg}(n)=F(-n)G(n)+F(n)G(-n)$$

and

$$\psi_{fg}(m,n)=F(n-m)G(-n)+F(-n-m)G(n) \tag{9}$$

where f and g are any two variables while F and G are their corresponding Fourier transforms.

We define the kinetic energy at level p averaged between the two latitudes $\phi_1=30°$ N. and $\phi_2=80°$ N. and around the earth as

$$K=\left\{\frac{\overline{|\mathbf{V}|^2}^{\lambda}}{2g}\right\}^{\phi}. \tag{10}$$

Similarly, the contribution A of an arbitrarily thick atmospheric layer centered at pressure p to the available potential energy of the whole atmosphere is given as

$$A=\frac{S}{g}\left\{\frac{\overline{\theta^{*2}}^{\lambda}}{2}\right\}^{\phi} \tag{11}$$

where

$$S=-\left(\frac{p}{p_0}\right)^{\kappa}\frac{R}{p}\left(\frac{\partial}{\partial p}\left\{\bar{\theta}^{\lambda}\right\}^{\phi}\right)^{-1}.$$

Both K and A may be partitioned in their zonal and eddy modes, respectively, as

$$K=\left\{\frac{\overline{\mathbf{V}}^{\lambda 2}}{2g}\right\}^{\phi}+\sum_{n=1}^{\infty}KE(n); \tag{12}$$

then

$$K=KZ+KE. \tag{13}$$

Similarly,

$$A=S\left\{\frac{\overline{\theta''^2}^{\lambda}}{2g}\right\}^{\phi}+\sum_{n=1}^{\infty}AE(n); \tag{14}$$

then

$$A=AZ+AE. \tag{15}$$

The formal expansion of the time rate of change of these four energy modes are given by equations (1) to (4) in the main text. The terms in these equations are now expanded and valid over a layer whose thickness is 1 mb:

$$CK=\sum_{n=1}^{\infty}CK(n)=\sum_{n=1}^{\infty}\left[\frac{-1}{g}\left\{\Phi_{uv}(n)\frac{\cos\phi}{a}\frac{\partial}{\partial\phi}\left(\frac{\bar{u}^{\lambda}}{\cos\phi}\right)\right\}^{\phi}\right], \tag{16}$$

$$CA=\sum_{n=1}^{\infty}CA(n)=\sum_{n=1}^{\infty}\left[\frac{-S}{g}\left\{\frac{1}{a}\frac{\partial\bar{\theta}''}{\partial\phi}\Phi_{v\theta}(n)\right\}^{\phi}\right], \tag{17}$$

$$CZ^*=\frac{S}{g}\frac{\partial\{\bar{\theta}^{\lambda}\}^{\phi}}{\partial p}\{\bar{\omega}''\bar{\theta}''\}^{\phi}, \tag{18}$$

and

$$CE^*=\sum_{n=1}^{\infty}CE(n)^*=\sum_{n=1}^{\infty}\left[\frac{S}{g}\frac{\partial\{\bar{\theta}^{\lambda}\}^{\phi}}{\partial p}\{\Phi_{\omega\theta}(n)\}^{\phi}\right]. \tag{19}$$

The geopotential flux convergences between the upper pressure level p_1 and lower pressure level p_2 are

$$BGE=\sum_{n=1}^{\infty}BGE(n)=\{\Phi_{\omega z}(n)\}^{\phi}\Big|_{p_2}^{p_1} \tag{20}$$

and

$$BGZ=\{\bar{\omega}''\bar{z}''\}^{\phi}\Big|_{p_2}^{p_1}. \tag{21}$$

The nonlinear redistribution of kinetic energy into the wave number n component from the other components is given by

$$LK(n)=\frac{1}{g}\left\{\sum_{\substack{m=-\infty\\ m\neq 0}}^{\infty}U(m)\left[\frac{1}{a\cos\phi}\psi_{uu_\lambda}(m,n)+\frac{1}{a}\psi_{vu_\phi}(m,n)-\frac{\tan\phi}{a}\psi_{uv}(m,n)\right]+V(m)\left[\frac{1}{a\cos\phi}\psi_{uv_\lambda}(m,n)+\frac{1}{a}\psi_{vv_\phi}(m,n)+\frac{\tan\phi}{a}\psi_{uu}(m,n)\right]\right\}^{\phi}. \tag{22}$$

The nonlinear redistribution of available potential energy into the wave number n component from the other

components is given by

$$LA(n)=\frac{S}{g}\left\{\sum_{\substack{m=-\infty\\ m\neq 0}}^{\infty} Q(m)\left[\frac{1}{a\cos\phi}\psi_{u\theta_\lambda}(m,n)+\frac{1}{a}\psi_{v\theta_\phi}(m,n)\right]\right\}^{\phi}. \quad (23)$$

ACKNOWLEDGMENTS

The author wishes to thank Prof. B. W. Boville for providing him the opportunity to investigate the problem studied above, Drs. J. Derome and I. Rutherford for critically reviewing the original text and suggesting many improvements, and the Meteorological Service of Canada for the support and the approval of this publication.

REFERENCES

Boville, B. W., Wilson, C. V., and Hare, F. K., "Baroclinic Waves in the Polar-Night Vortex," *Journal of Meteorology*, Vol. 18, No. 5, Oct. **1961**, pp. 567–580.

Brown, J. A., Jr., "A Diagnostic Study of Tropospheric Diabatic Heating and the Generation of Available Potential Energy," *Tellus*, Vol. 16, No. 3, Aug. **1964**, pp. 371–388.

Charney, Jule G., "On a Physical Basis for Numerical Prediction of Large-Scale Motions in the Atmosphere," *Journal of Meteorology*, Vol. 6, No. 6, Dec. **1949**, pp. 371–385.

Charney, Jule G., and Drazin, P. G., "Propagation of Planetary-Scale Disturbances From the Lower Into the Upper Atmosphere," *Journal of Geophysical Research*, Vol. 66, No. 1, Jan. **1961**, pp. 83–109.

Gates, W. Lawrence, "Static Stability Measures in the Atmosphere," *Journal of Meteorology*, Vol. 18, No. 4, Aug. **1961**, pp. 526–533.

Godson, Warren L., and Wilson, C. V., "The Structure of the Arctic Winter Stratosphere Over a Ten Year Period," *Canadian Meteorological Memoirs*, Meteorological Branch, Department of Transport, Toronto, Nov. 11, **1963**, 193 pp.

Holopainen, Ero E., "On the Dissipation of Kinetic Energy in the Atmosphere," *Tellus*, Vol. 15, No. 1, Feb. **1963**, pp. 26–32.

Krueger, Arthur F., Winston, Jay S., and Haines, Donald A., "Computations of Atmospheric Energy and Its Transformation for the Northern Hemisphere for a Recent Five-Year Period" *Monthly Weather Review*, Vol. 93, No. 4, Apr. **1965**, pp. 227–238.

Lorenz, E. N., "Available Potential Energy and the Maintenance of the General Circulation," *Tellus*, Vol. 7, No. 2, May **1955**, pp. 157–167.

Muench, H. Stuart, "Stratospheric Energy Processes and Associated Atmospheric Long-Wave Structure in Winter," *Environmental Research Papers* No. 95, Air Force Cambridge Research Laboratories, Hanscom Field, Bedford, Mass., Apr. **1965**, 120 pp.

Murakami, Takio, and Tomatsu, Kiichi, "The Spectrum Analysis of the Energy Integration Terms in the Atmosphere," *Journal of the Meteorological Society of Japan*, Ser. 2, Vol. 42, No. 1, Feb. **1964**, pp. 14–25.

Paulin, Gaston, "Spectral Atmospheric Energetics During January 1959," *Arctic Meteorology Research Group Publication in Meteorology* No. 91, Department of Meteorology, McGill University, Montreal, Quebec, Canada, June **1968**, 328 pp.

Paulin, Gaston, "A Simplified Method of Computing Stratospheric Heating Rates and Associated Generation of Available Potential Energy," *Monthly Weather Review*, Vol. 97, No. 5, May **1969**, pp. 359–370.

Perry, J. S., "The Energy Balance During a Sudden Stratospheric Warming," Ph. D. thesis, University of Washington, Seattle, Apr. **1966**, 185 pp.

Rutherford, Ian D., "The Vertical Propagation of Geostrophic Waves in a Low-Order Spectral Model," *Arctic Meteorology Research Group Publication in Meteorology* No. 92, Department of Meteorology, McGill University, Montreal, Quebec, Canada, July **1969**, 122 pp.

Saltzman, Barry, "Equations Governing the Energetics of the Larger Scales of Atmospheric Turbulence in the Domain of Wave Number," *Journal of Meteorology*, Vol. 14, No. 6, Dec. **1957**, pp. 513–523.

Saltzman, Barry, and Teweles, Sidney, "Further Statistics on the Exchange of Kinetic Energy Between Harmonic Components of the Atmospheric Flow," *Tellus*, Vol. 16, No. 4, Nov. **1964**, pp. 432 435.

Scherhag, Richard, "Die explosionsartigen Stratosphärenerwarmungen des Spätwinters 1951/1952" (The Explosion-Like Stratospheric Warmings of the Late Winter 1951/1952), *Berichte Duetscher Wetterdienst in der U.S.-Zone* No. 38, Germany, **1952**, pp. 51–63.

Steiner, Harold A., "The Stratospheric Wind Regimes of the 1958–59 Winter: 80 W Cross Sections: Sea-Level to 35 Km," *Arctic Meteorology Research Group Publication in Meteorology* No. 41, Department of Meteorology, McGill University, Montreal, Quebec, Canada, Apr. **1961**, 106 pp.

Vernekar, Anandu D., "On Mean Meridional Circulations in the Atmosphere," *Monthly Weather Review*, Vol. 95, No. 11, Nov. **1967**, pp. 705–721.

Wiin-Nielsen, A., "On Energy Conversion Calculations," *Monthly Weather Review*, Vol. 92, No. 4, Apr. **1964**, pp. 161–167.

Yang, Chien-Hsiung, "Non-Linear Aspects of the Large-Scale Motion in the Atmosphere," Report ORA–08759–1–T, Grant NSFGA–10947, College of Engineering, Department of Meteorology and Oceanography, University of Michigan, Ann Arbor, Nov. **1967**, 173 pp.

Yang, Chien-Hsiung, "A Diagnostic Study on Non-Linear Energy Exchanges Among Harmonic Components in the Atmosphere," *Arctic Meteorology Research Group Publication in Meteorology* No. 90, Department of Meteorology, McGill University, Montreal, Quebec, Canada, Mar. **1968**, pp. 85–86.

[*Received January 21, 1970; revised April 8, 1970*]